Title

Ion and organic transport in Graphene oxide membranes: Model development to difficult water remediation applications.

Authors

Aher, Ashish

Nickerson, Trisha

Jordan, Clair

et al.

Publication Date

2020-06-01

DOI

10.1016/j.memsci.2020.118024

Peer reviewed

HHS Public Access

Author manuscript

J Memb Sci. Author manuscript; available in PMC 2022 July 29.

Published in final edited form as:

J Memb Sci. 2020 June 01; 604: . doi:10.1016/j.memsci.2020.118024.

Ion and organic transport in Graphene oxide membranes: Model development to difficult water remediation applications

Ashish Aher[a], **Trisha Nickerson**[a], **Clair Jordan**[b], **Fox Thorpe**[a], **Evan Hatakeyama**[c], **Lindell Ormsbee**[d], **Mainak Majumder**[e,f], **Dibakar Bhattacharyya**[a,*]

[a]Department of Chemical and Materials Engineering, University of Kentucky, Lexington, KY, USA

[b]Department of Engineering, Smith College, Northampton, MA, USA

[c]Chevron Corp., Richmond, CA, USA

[d]Department of Civil Engineering, University of Kentucky, Lexington, KY, USA

[e]Nanoscale Science and Engineering Laboratory (NSEL), Department of Mechanical and Aerospace Engineering, Monash University, Clayton, Australia

[f]ARC Research Hub on Graphene Enabled Industry Transformation, Monash University, Clayton, Australia

Abstract

The role of steric hindrance and charge interactions in governing ionic transport through reduced graphene oxide (rGO) and commercial (DOW-Filmtec NF270) membranes was elucidated by a comprehensive study of experimental and established mathematical analysis based on Nernst-Planck equation. A charge-dominated salt exclusion mechanism was observed for the rGO membranes, which exhibited retention from low (7%) to moderate (70%) extent depending on the nature of ions (5 mM). Swelling of GO (1.2 nm interlayer distance) in water beyond the hydrated diameter of ions was attributed as a primary cause for lowering steric hindrance effects. The influence of parameters affecting charge interactions, such as pH and ionic strength, on the extent of salt rejection was modelled. The potential impact of the membrane's charge density, GO loading and interlayer spacing on salt retention was quantified by performing sensitivity analyses. For a high TDS produced water sample, the rGO membranes partially retained divalent cations (Ca:13%) and exhibited high dissolved oil rejection. The membranes were found to be suitable for the treatment of high TDS water with the goal of selectively removing organic impurities, and thus minimizing the impact of osmotic pressure effect. Performance of the membranes was also investigated for retention of water remediation related organic anions, using perfluoro octanoic

*Corresponding author. Chemical and Materials Engineering, 177 FPAT Bldg., University of Kentucky, Lexington, KY, 40506, USA., db@uky.edu (D. Bhattacharyya).

CRediT authorship contribution statement

Ashish Aher: Writing - original draft. **Trisha Nickerson:** Writing - review & editing, Writing - review & editing. **Clair Jordan:** Data curation. **Fox Thorpe:** Data curation. **Evan Hatakeyama:** Writing - review & editing, **Mainak Majumder:** Writing - review & editing. **Dibakar Bhattacharyya:** Conceptualization, Writing - original draft, Writing - review & editing.

Declaration of competing interest

The authors have no competing interests to declare.

Appendix A. Supplementary data

Supplementary data to this article can be found online at https://doi.org/10.1016/j.memsci.2020.118024.

(PFOA) acid as a model compound. rGO membranes exhibited a charge-dominated exclusion mechanism for retention (90%) of PFOA (1 ppm).

Keywords

Reduced graphene oxide; Nanofiltration; Nernst-Planck; Produced water; Perfluoro octanoic acid (PFOA)

1. Introduction

Graphene oxide (GO) has garnered vast interest of the membrane community for aqueous and organic solvent nanofiltration applications [1–4]. GO membranes are known to provide a highly tunable platform and extensive reports exist displaying nanofiltration performance ranges from low to high salt retention [3,5–7]. Desalination performance by nanofiltration membranes is sensitive to various operating conditions, such as water flux, operation pH, temperature, feed ionic strength, etc. Therefore, it is necessary to account for these parameters during performance evaluation or comparison of various GO-based membranes.

Commercially available polymeric nanofiltration membranes are known to govern exclusion of ions by three mechanisms including dielectric exclusion, charged-based exclusion and steric hindrance [8]. Ion transport limited by steric hindrance depends on the effective pore size of the membranes, whereas, charged-based exclusion depends on the charge density of the active separation layer. The same principles can be extended to analyze ionic transport through GO membranes. However, GO-based membranes differ from polymeric nanofiltration membranes in a few ways. Transport of water through GO membranes is believed to occur through the spacing of the gallery between the deposited GO sheets [9]. A significant expansion of several angstroms is observed in the interlayer gallery spacing of GO by adsorbing water molecules [10]. Furthermore, expansion in interlayer gallery spacing depends on the oxidation extent of the GO: partially reduced GO channels expands to a lesser extent as compared to pristine GO in an aqueous environment [11]. The impact of steric hindrance on total ionic transport, which depends on the dimensions of the pore size/interlayer gallery spacing, is expected to decrease with the expansion of interlayer gallery spacing.

In addition, GO is characterized by a non-homogeneous distribution of oxygenated functionalities along the edge defects of the sheets surrounding the sp2 hybridized domains, which differentiates these membranes from regular polymeric nanofiltration membranes. Additionally, the path length for water transport through these sheets is large, and depends on the size of individual GO sheets and GO loading [12]. Changes in the diffusive path length affects the effective resistance for ion transport, and needs to be considered while evaluating and/or comparing the membrane performance [12].

Approaches based on an extended Nernst-Planck equation are very popular in modeling ionic transport through nanofiltration membranes [8]. Briefly, a Nernst-Planck's approach considers three different modes for transport of ions through the membrane via hindered diffusion, convective coupling, and potential gradient. Hindered diffusion and convective

coupling of ions is a function of effective pore size or interlayer spacing in the case of GO membranes [13]. As one would expect, with a smaller pore size, ions experience a higher hindrance to diffusion and a lower convective coupling. The potential gradient across the membrane occurs due to the presence of charge functionalities and has a dependence on feed conditions such as valency of ions and ionic strength of feed. Therefore, rejection by nanofiltration is sensitive to these feed conditions. In addition, studies have also extended this approach to account for partitioning of ions based on steric hindrance and dielectric exclusion. A model based on the Nernst-Planck equation would thus enable quantification, comparison and modelling of the performance of GO-based membranes under a wide set of parameters.

Among the advancing frontiers in membrane-based separations, a key area of interest exists in the selective separations of organics (300–1000 Da) from water containing high amounts of dissolved salts [14]. State of the art reverse osmosis membranes are a popular choice for desalination of water and removal of micropollutants. However, in the case of the treatment of water containing high total dissolved solids (TDS), it is essential to use membranes with low retention of inorganic salts to avoid a high osmotic pressure gradient. Selective separations of organics from high TDS water (such as, produced water) is a key element in determining separation efficiency. GO-based membranes could be effectively used for produced-water streams to remove dissolved oily components. GO-based membranes are less prone to fouling from oily components owing to the hydrophilic nature of GO, giving it an edge over polymeric membranes [15]. Common organic impurities, such as naphthenic acids, are negatively charged with a molecular weight ranging from 200 to over 500 [16]. One could anticipate higher retention of these impurities owing to charge-based repulsion forces in conjunction with steric hindrance.

The rGO membranes being negatively charged, could also retain organic anions from water, such as perfluoro octanoic acids (PFOA). PFOA is a surfactant like molecule which has a negatively charged carboxylate group on a perfluorinated carbon backbone. This organic molecule has gained concern owing to its tendency due to bioaccumulation and toxicity [17,18]. Nanofiltration has achieved high removal efficiency (up to 90% at 1 ppm feed concentration level) and thus, has allowed high recovery of purified water [19]. One desired aspect of nanofiltration for treatment of PFOA contaminated water is to have selective removal of these molecules and letting the salts pass through the membrane [18]. Selective separation would minimize salt precipitation and also, purified water can retain the essential minerals. As the rGO membranes are known to have lower salt retention, they serve as a potential candidate for remediation of PFOA.

In this study, we provide an understanding of the underlying mechanism for ion transport through GO-based membranes with the aid of the extended Nernst-Planck equation. Objectives of this study were: 1) to study the role of steric hindrance and convective coupling along with charge-based interactions for the transport of ions through rGO membranes under a wide set of operating conditions, 2) to examine the potential application of GO membranes for partial hardness removal from high TDS produced water and to study membrane fouling and oil removal by rGO membranes in the presence of small amounts of dissolved oil, and 3) to investigate the removal of environmentally

important perfluoro organic anion (PFOA), and develop an understanding of the underlying exclusion mechanism. To quantify the impact of operating conditions such as recovery, feed concentration and pH.

2. Experimental section

2.1. Materials

Graphene oxide (Trade name: Graphenea Graphene oxide) was purchased from Graphenea, Inc. Sodium sulfate (Na_2SO_4), Sodium chloride (NaCl) Magnesium sulfate ($MgSO_4$), Magnesium Chloride ($MgCl_2$), Sulfuric acid (H_2SO_4), Sodium hydroxide (NaOH) and Potassium chloride (KCl) were purchased from VWR. The PVDF substrate used in the study was a PV200 membrane with an effective pore size of 110 nm, obtained from Nanostone-Water Co. Produced water samples were provided by Chevron Corp. Sample was collected in the process after solids and oil separation including gravity separation, and induced gas floatation. The samples were allowed to settle in the laboratory for an extended period. It is expected that most the dispersed oil was removed; however, testing for submicron oil droplets was not conducted. It is possible that some of the dissolved organics may be finely dispersed droplets. Reagent grade perfluorooctanoic acid (PFOA, 97% purity) was purchased from Alfa Aesar (lot# 10212100). Water used at all stages of the experiments was purified (final resistivity <18.2 MΩ, TOC<1 ppb) using a Purelab flex water purifier obtained from ELGA Lab water. All reagents used in the study were of reagent grade and were used as received.

2.2. Membrane synthesis

The method for rGO membrane synthesis used in this study is similar to one employed in our earlier reported research [20]. The only difference between the two synthesis procedures was the amount of GO deposited on the polymeric substrate. Briefly, a wire wound rod (wet film thickness: 7.7 μm) was used to cast an aqueous dispersion of GO on the substrate (dimensions: 10 cm × 20 cm). Four coating cycles were employed for membrane synthesis with intermediate air drying of the deposited films between each cycle. Casting was done manually using an aqueous dispersion of GO (2 mg/ml). Each coating cycle corresponded to 15 mg/m^2 of GO loading. After achieving a loading of 60 mg/m^2 (with four coating cycles), the GO-loaded substrate was thermally reduced at 90 °C for 24 h.

2.3. Performance evaluation in cross-flow mode of operation

Membrane performance was evaluated in a cross-flow filtration cell, operated at 25 °C and 0.5 Pa shear rate. DI water was passed through the membrane at 50 psi for 12 h, before monitoring its performance parameters. A schematic of the experimental setup and operational details can be found in SI section 1. Flux was recorded by measuring the mass of permeate collected over a measured time period (at least 5 min). Concentration of single salt solution was measured by monitoring the conductivity of the salt solution using a (Fisher Scientific 09–330 Traceable Bench) conductivity meter. To measure sodium sulfate flux at different pH values, the feed pH was initially lowered to 3 by H_2SO_4 and was raised gradually by adding NaOH. The rejection (R) formula is defined in Equation (1).

$$R(\%) = \left(1 - \frac{C_{per}}{C_{feed}}\right) \times 100 \quad (1)$$

C_{per} is the concentration of permeate and C_{feed} is the concentration of feed solution.

Retention of organic anion, PFOA, was operated at a different feed recovery in a dead-end mode of operation. Feed recovery in this study is defined as the volume fraction of feed recovered as permeate from membrane filtration.

2.4. Solute permeability analysis using diffusion cell

Diffusive transport of a species across the membrane was quantified using an automated system, ILC07, obtained from PermeGear. A flow diagram and operational details of the diffusion cell are provided in SI section 2. Additional details about the operation of the instrument can be found elsewhere [21]. The system was equipped with 7 flow diffusion cells assembled in a parallel configuration, a high precision peristaltic pump with an adjustable operational flow rate ranging from 10 μl/min to 770 μl/min, a temperature control unit and an automated fraction collector. Diffusion cells consisted of a donor chamber (1 cc volume) and collector chamber. The collector chamber was circulated with carrier phase (solution media) using a high precision pump, and the solution leaving the collector chamber was collected in sampling vials using an automated fraction collector. Concentrations of a species in sampling vials were then measured separately to determine the diffusive flux of the species. The concentration of the species at various time intervals in the collector chamber was correlated with solute permeability by Equation (2).

$$C_{collector}(t) = \frac{A \times B \times C_{donor}(t0)}{F_{media}} \times exp\left(\frac{-A \times B \times t}{V_{donor}}\right) \quad (2)$$

Variables B, A, $C_{donor}(t)$, $C_{collector}(t)$, F_{media}, V_{donor} and $C_{donor}(t_0)$ are solute permeability, membrane area, the concentration of donor and collector chamber, flow rate of media (110 μl/min) being circulated in the collector chamber, volume of the donor chamber (800 μl) and initial concentration of the donor chamber, respectively.

2.5. Analytical protocols

For single salt solutions, the concentration of the salts was determined using a conductivity probe (Fisher Scientific 09–330 Traceable Bench). Calibration curves up to 500 ppm with around 5 standards were created to determine salt concentration from conductivity measurements. Analysis of mixed salt solutions was done using inductively coupled plasma-optical emission spectroscopy (ICP-OES Agilent 700). Analysis of anions was performed using ion-exchange chromatography (Thermo Scientific Dionex). The concentration of humic acids, various dyes and aromatic compounds used for quantifying separation performance of the membrane were analyzed using a UV-VIS spectrometer (VWR UV-6300PC). Organic content of the water was analyzed using a total organic carbon analyzer (Shimadzu TOC 5000).

Dissolved oil concentrations were determined by the oil extraction method [22,23]. Produced water samples were pre-filtered with filter paper (pore size: 200 μm) before each experiment to remove suspended solids. For extraction, 35 ml of analyte solution was extracted with 5 ml of AK225 solvent at pH 2. The concentration of oil in the solvent phase was measured using a Duratech DTIR 970 analyzer. DTIR is an infra-red analyzer used to measure the infrared energy transmitted through the sample at a single wavelength (1650 cm^{-1}).

Perfluorooctanoic acid (PFOA) analysis was carried out by the following EPA method 537. A UPLC/MS/MS system (Varian ProStar 1200L) equipped with a C18 column and quadrupole mass spectrometer was used for analysis of PFOA. Gradient elution of 20 mM ammonium acetate (A) and pure methanol (B) was used as a carrier phase with a flow rate of 0.8 ml/min. Initial and final mobile phase composition (after 12 min) were 40% (of A by vol.) and 95% (of A by vol.).

3. Performance evaluation using extended Nernst-Planck equation

A detailed review on the modelling approach based on the Nernst-Planck equation can be found elsewhere [8,24]. In this study, ionic transport though the membrane was modelled using Equation (3). The computation approach used to solve the equations is similar to the one described by Maria et al. [25].

$$J_i = -K_{di}D_i\frac{dC_i}{dx} + K_{ic}C_iJ_v - \frac{Z_iC_iD_iF}{RT}\frac{d\phi}{dx} \quad (3)$$

Variables J_i, D_i, J_v, K_{ci}, K_{di}, and $d\Psi$, are the species flux, diffusion coefficient, water flux, convective coupling coefficient, hindered diffusion coefficient and Donnan potential, respectively.

The first term in Equation (3) accounts for diffusive transport through the membrane, where K_d is the hindered coefficient for ion diffusion. The second term represents convective transport of ions through the membrane in which Kc is the coupling coefficient. K_d and K_c are dependent on the ratio of ionic radius to effective pore size (λ_i) of the membrane and can be estimated by equations (4) and (5) [26].

$$K_{di} = 1.0 - 2.30\lambda_i + 1.154\lambda_i^2 + 0.224\lambda_i^3 \quad (4)$$

$$K_{ci} = 1.0 + 0.054\lambda_i - 0.988\lambda_i^2 + 0.441\lambda_i^3 \quad (5)$$

The variable $\lambda_i = r_i/r_p$ (ionic radius/pore radius).

There is no net current flow through the membrane, as in no net flux of charge crosses the membrane. Therefore, in order to account for the transport of cationic species through the negatively charged GO membranes, the model incorporates a potential gradient term (third

term in Equation (3)). This term can be estimated by Equation (6), which is derived from Equation (3) using the condition that there is no net charge flux across the membrane.

$$\frac{d\phi}{dx} = \frac{\sum_{i=1}^{n} \frac{z_i J_v}{K_{id} D_{i\infty}} \left(K_{ci} C_i - C_{i\_permeate}\right)}{\frac{F}{RT} \sum_{i=1}^{n} z_i^2 C_i} \quad (6)$$

In this computation, the membrane was assumed to have a fixed charge density, X_d, across its thickness and a condition of electro neutrality was used at each node as expressed in Equation (7).

$$\sum_{i=1}^{n} z_i C_i + X_d = 0 \quad (7)$$

Steric partitioning was also accounted for in the model and the partitioning coefficient of various ions at the membrane surface was calculated using Equation (8) [27].

$$\varphi = (1 - \lambda_i)^2 \quad (8)$$

Concentration of ions in the permeate was calculated by Equation (9).

$$C_p = J_i / J_v \quad (9)$$

In this study, values of effective pore radius for Graphene Oxide and NF270 membranes were obtained from our earlier reported size exclusion study and literature value, respectively [28,29]. Values of effective charge density (Xd) and diffusion length used in the model were optimized to fit the experimental data. The parameters were optimized with an objective function of minimizing root mean square deviation between experimental and computed values. For a given water flux (Jv), ionic flux through the membrane was computed using Equations (3) and (6), and by imposing the constraint of electro neutrality.

4. Results and discussion

GO membranes used in this study are similar to the ones used in our earlier reported research [20,28]. In this section, membrane characterization and the change in physiochemical properties of GO during thermal reduction is discussed first. Salt retention performance of GO and polymeric (DOW-NF270) membranes is quantified for different types of salts under various operating conditions (operating flux, ionic strength, pH) and is assessed using an extended Nernst-Planck equation. Later in this section, the membrane performance is discussed for the treatment of high TDS produced water streams with the objective of partial hardness and dissolved oil removal. Finally, the performance of GO and commercial nanofiltration membranes for removal of an emerging organic pollutant (PFOA)

is discussed with an impetus for elucidating the role of charge in the underlying exclusion mechanism.

4.1. Characterization

Detailed characterization of the rGO membranes used in this study can be found in our earlier reported research [20,28]. GO sheets used in this study for membrane synthesis had an average lateral dimension of 1.7 μm (±0.9 μm), as determined using AFM. Membranes had an average GO thickness of 70 nm and a root mean square surface roughness of 78 nm [20].

During membrane synthesis, GO was partially reduced by employing thermal incubation. Characterization of GO after thermal incubation is important for this study, as physiochemical properties of GO sheets determine the surface hydrophilicity and interlayer spacing, and these properties are vital to the permeability-selectivity of GO membranes. Heat treatment of GO at 90 °C resulted in a decline in the O/C (Oxygen/Carbon) ratio from 0.46 to 0.37 after 24 h of incubation. C1s binding energies of the GO measured using XPS showed a significant reduction in relative intensity of the peak corresponding to C–O binding energies (286.8 eV), suggesting a loss of hydroxyl functionalities. FTIR characterization of the membrane also revealed a decline in relative intensity at wavenumbers corresponding to epoxy (1100 cm^{-1}) and hydroxyl (2700–3300 cm^{-1}) functionalities, further confirming the loss of these functionalities from GO sheets. Loss of oxygen containing functionalities resulted in an increase in hydrophobicity of the membrane. Contact angle of the membrane surface with water increased from 33° to 79° after thermal incubation [20].

Interlayer spacing between GO sheets acts as a primary route for transport of molecules across the GO layers, and thus is critical for governing performance of the membrane. Spacing is governed by the equilibrium between two competing forces: attractive van-der walls forces and repulsive electrostatic repulsive forces. sp2 domains on GO sheets are partially restored during thermal incubation, which increases the intensity of attractive van-der-wall forces and results in a decrease in the interlayer spacing. In our previous study, we observed a decrease in interlayer spacing from 1.25 nm to 0.85 nm (in the dry state) after thermal incubation [28].

4.1.1. Surface potential—Performance of nanofiltration membranes is significantly driven by the charge density of functional groups and the effective pore size of the membrane. One effective way to characterize the charge density of functional groups is through surface potential measurements. Potential on the membrane surface is caused by the formation of an electrical double layer and is dependent on the surface functional groups and their response to feed conditions, such as pH and salt type. GO sheets, being decorated with carboxylate groups, has a negative surface potential at neutral pH. Surface potential of the membrane measured for a range of pH values is shown in Fig. 1. Surface potential of the GO membranes was −24 mV at pH 7, which declined to −13 mV at pH 3. The decrease in surface potential at lower pH is expected due to protonation of carboxylate groups. Even at

pH of 3.5, significant negative potential was observed suggesting only partial protonation of carboxylate groups.

4.2. Pure water permeability

Initially, membrane performance was quantified by measuring the response of pure water flux to the operating pressure gradient across the membrane. Membranes with different GO loadings and commercial nanofiltration membranes (DOW FILMTEC NF270) were tested for water permeability. All membranes exhibited a proportional flux increase with the applied pressure gradient over the investigated range up to 13 bars (Fig. 2). The permeability of GO-based membranes was inversely proportional to the amount of GO coated on the substrate. The resistance of GO layers is expected to dominate the overall resistance for flow through the membrane [30]. The performance can be analyzed by a resistance in series approach, revealing that the resistance of the GO layer increases linearly with the amount of GO coated on the substrate (SI section 3). Analysis yielded a specific resistance of 0.0016 bar/LMH per mg/m^2 loading of GO (resistance offered by unit amount of GO deposited on substrate). The specific resistance offered by the deposited GO layer is a function of its chemical composition and the alignment of GO sheets [5]. Akbari et al. have demonstrated that resistance of the GO layer can be lowered significantly by aligning GO sheets [31]. Ideally, an ultrathin and aligned layer of GO comprised of only a few GO sheets is desired to achieve high performance. However, the underlying substrate has some intrinsic surface roughness, and therefore, necessitates a minimum thickness of GO layer to ensure defect free coating of GO. Our attempts to synthesize membranes with a GO layer coating less than 18 mg/m^2 yielded membranes with poor separation performance as quantified by neutral red dye (probe molecule, size: 1.2 nm) retention.

4.3. Dependence of retention on the nature of salts

The role of charge and steric hindrance in the underlying transport mechanism of ions through GO membranes can be quantified by measuring retention of different salts at a range of operating pressure gradients. Before performing salt retention tests, membranes were tested for defects by measuring the Neutral Red dye retention (Size: 1.2 nm). High retention of dye (>95%) was observed for both the membranes indicating the absence of microstructural defects. In this study, four different salts (NaCl, Na_2SO_4, $MgCl_2$, and $MgSO_4$) were used to quantify the retention performance of rGO membranes. Control runs were performed with NF270 membranes. These salts differ in terms of hydration radius, nature of charge and charge density. Magnesium has a larger hydrated radius compared to sodium (Table 1) [32]. Also, Magnesium and sulfates are divalent and have higher charge densities. These ions are, therefore, expected to experience higher charge interaction forces with the membrane. In typical commercial nanofiltration membranes, the pore size of the membranes is close to the hydration radii of divalent ions and a significant steric hindrance occurs to the transport of these ions [33,34]. As a result, for commercial nanofiltration membranes, salts containing divalent ions have higher retention compared to ones containing monovalent ions.

The retention of the four salts tested at different operating pressure gradients by rGO and NF270 membranes is shown in Fig. 3a and b, respectively. The order of retention of the four

salts by rGO was Na_2SO_4>$MgSO_4$>NaCl > $MgCl_2$ and the trend was found consistent with literature [30]. The control test conducted with the NF270 membrane showed the order of retention for investigate salts as $MgSO_4$≈Na_2SO_4>$MgCl_2$>NaCl. Salt permeabilities through rGO and NF270 membranes were evaluated in a diffusion mode using single salt solutions at a feed concentration of 20 mM (Fig. 3b, c, e and f). Trends in salt permeabilities were consistent with the rejection data.

It is interesting to note that rGO membranes showed higher rejection of sodium salts compared to magnesium salts with the same counter ions, whereas, NF270 membranes exhibited an different trend for the two salts. In the case of ionic transport through nanopores, ions are sterically hindered when the dimensions of the pores approach the hydrated ionic radius, causing an energy barrier for ionic transport. The proportional contribution of steric effects to the overall activation energy for ionic transport is high when the pore size of the membrane approaches the hydration radius of ions, resulting in less significant charge-based interactions for governing ionic transport. For example, through molecular dynamic simulations, Richards et al. showed that the contribution of charge-based interactions (pore surface charge density: 0.1 C/m^2) is only 14% of the overall activation energy (31.6 kcal/mol) barrier for transport of fluoride ions through a membrane with an effective pore radius of 0.34 nm [34]. In contrast, for pore radii larger than the ion's hydrated radius, the fractional contribution to the total energy barrier due to ion dehydration is small compared to charge-based contributions [3,34]· Therefore, performance of membranes with pore radius significantly larger than hydrated ion radius is expected to be driven by charge interactions. One could further improve the accuracy of the model by incorporating a partitioning term based on the dehydration effects using a solvation energy barrier. In the current investigation, the effective pore radius of GO membranes was around 0.6 nm, significantly greater than the hydration radius of ions, and therefore, dehydration of ions is expected to have relatively less contribution to the overall energy barrier for retention of ions.

rGO, being hygroscopic, adsorbs water molecules on its basal plane depending on the extent of oxidation. In our earlier study, we observed an increase in interlayer spacing from 0.8 nm in the dry state to more than 1.2 nm in the wet state due to water sorption in the rGO domain [28]. Whereas, the cross-linked polyamide network of a commercial NF270 membrane is reported to have a relatively smaller effective pore size (diameter) of 0.87 nm [29]. One would, therefore, expect higher steric hindrance for salt transport through a NF270 membrane compared to an rGO membrane. As hydration radius of magnesium ions is larger than sodium ions, magnesium salts are sterically hindered to a greater extent compared to sodium salts by the NF270 membrane. In the case of rGO membranes, the channel width (or effective pore size) is significantly larger than the hydrated radius of both sodium and magnesium ions. Therefore, steric effects are less significant, and divalent magnesium cations are partitioned more favorably compared to monovalent sodium cations in the negatively charged GO domain. Also, sulfate ions experience the highest repulsive forces among the four investigated ions and as a result, higher retention of sulfate salts was observed compared to chloride salts. This is a clear indication that salt exclusion by rGO membranes is due to a charge-driven mechanism, whereas, exclusion by NF270 membranes is governed by both charge and steric effects.

Parameters of the extended Nernst-Planck equation optimized for the two investigated membranes are summarized in Table 2. The effective pore opening of the rGO membranes was fixed at 1.2 nm, the pore size that was established in our previous study via retention of different solutes and XRD characterization [28]. Diffusion length and charge density of the membrane were optimized to fit the experimental data. For the NF270 membrane, the optimized pore opening was in close agreement with the literature value of 0.87 nm [29]. A notable difference in the diffusion length of the two investigated membranes was observed. The optimized diffusion length of rGO was almost 10 times the one optimized for the NF270 membrane. This result is intuitive as the rGO domain offers a highly tortuous path for the transport of ions through the membrane. Monte-Carlo simulations performed on the structure of GO laminates by Ritt et al. estimated the tortuosity (effective length/membrane thickness) of the membrane to range from 970 to 1400 (dimensionless) [35]. Also, despite the fact that rGO membranes have larger pore openings, their lower membrane permeabilities compared to NF270 membranes suggests that molecules traverse longer diffusion lengths across the GO laminates. Since charge interactions were the primary source of resistance for ionic transport through rGO membranes, the optimized value of effective charge density of the rGO membrane was higher than the NF270 membrane. It should be noted that charged groups are primarily present in edges of GO sheets (in contrast to NF270), which could be one of the reasons for higher effective charge density of the membrane [36].

4.4. Role of pH

Monitoring salt retention of GO membranes at different pH values provides an opportunity to further quantify the impact of charge on the underlying transport mechanism. Zeta potential measured for the rGO membrane at different pH values showed a decline from −24 mV at pH 7 to −13 mV at pH 3. Since co-ions have to overcome the surface potential barrier, the tendency of salts to partition into the membrane domain is expected to increase at lower a pH, resulting in a higher ionic flux through the rGO membrane. GO membranes showed a constant water flux of 13.8 LMH over the investigated range of pH values at 7 bar, suggesting that the effective interlayer spacing was not significantly altered. Therefore, upon lowering pH, steric hindrance for the ionic transport is not likely to be impacted and any change in ionic transport across the rGO membrane will be primarily due to alterations in charge-based interactions. Fig. 4 shows a decrease in rejection of Na_2SO_4 for a pH below 4 at a given water flux. In an effort to maintain constant ionic strength during the course of the experiment, the pH of Na_2SO_4 solution was initially lowered using sulfuric acid and was, then, gradually increased by adding NaOH during the experiment.

For modelling the performance of the membrane, charge densities were estimated at different pH values using surface zeta potential values shown in Fig. 1. Initially, the ratio of charge density at varying pH values (SI Fig. S4) with reference to charge density at pH 7 were determined with the aid of the Grahame equation, as shown in Equation (10). Charge densities at different pH were obtained by multiplying the estimated ratio by the reference value of the optimized charge density at pH 7. The estimated response of the membrane at varying pH is shown in Fig. 4. Predicted salt retentions at acidic pH (4) were lower than experimental results.

$$\frac{X_{d\ @\ pH}}{X_{d\ @\ pH=7}} = \frac{\sinh\left(e\zeta_{@\ pH}/2K_BT\right)}{\sinh\left(e\zeta_{@\ pH=7}/2K_BT\right)} \quad \text{Equation 10}$$

The variables e, ζ, K_B and T are electron charge, surface zeta potential, Boltzmann constant and absolute temperature, respectively.

4.5. Impact of ionic strength

Ionic strength of the feed solution also plays a critical role in governing the surface potential arising from the electric double layer formed on charged surfaces. At higher ionic strength, the charge on the membrane surface is screened to a greater extent due to the abundance of counter ions in solution [37]. The decline in surface potential is more severe when higher valence counter ions are present in solution, owing to the formation of complexes by these counter ions with charged functionalities on the membrane surface. As a result, repulsive forces between co-ions and the membrane surface are weakened. The suppression of charge interactions at higher ionic strengths causes salt retention to decline [18,38,39].

The extent of salt retention decline for increased ionic strength, however, depends on the impact of charge in the overall exclusion mechanism of charged species by nanofiltration membranes [18,38]. The impact of feed ionic strength on ionic transport was quantified by measuring the retention of Na_2SO_4 by rGO membranes for feed concentrations of 1.5 mM and 6.8 mM. Retention was >90% for a 2 mM Na_2SO_4 feed at a water flux of 10 LMH (Fig. 5a). Rejection (50–70%) declined significantly when the feed concentration was increased to 5 mM. In a diffusion mode of operation, permeability of Na_2SO_4 was measured with an increasing feed concentration, up to 100 mM (Fig. 5b). As expected, permeability of Na_2SO_4 through the rGO membrane increased with increasing feed concentration. Na_2SO_4 permeability exhibited a power law dependence, with a permeability increase proportional to the 0.34th power of the feed concentration. The impact of ionic strength on the surface potential can also be predicted in terms of Debye length, which serves as a metric for the range over which electrostatic effect persists, and is inversely proportional to the square root of the ionic feed concentration. At a higher ionic strength, surface potential decreases, which, in turn, increases the partitioning of ions on the membrane surface and ionic flux through the membrane.

4.6. Sensitivity to effective charge density

GO membranes with various charge densities have been synthesized for nanofiltration applications. Charge density of GO membranes can be modulated by controlling the extent of oxidation of GO. In this study, a sensitivity analysis was performed to quantify the impact of charge density on the ionic transport through the membranes as shown in Fig. 6a. It can be noted that for the investigated set of parameters, at a higher charge density, the increase in Na_2SO_4 retention is less sensitive to an increase in charge density. The model was extended to analyze results published by Yuan et al. [5]. In the mentioned study, two GO membranes were synthesized with different extents of oxidation and had surface potentials of −38 mV and −52 mV at pH 7. Improved desalination performance was reported by the authors for membranes with higher oxidation extent. However, after

replotting the same rejection data against the operational water flux, as shown in Fig. 6b, it is evident that the desalination performance of both membranes is similar. One of the major differences between the two membranes was in the interlayer distance between the deposited GO sheets. Interlayer spacing for the GO with a lesser extent of oxidation was 1.36 nm, whereas, interlayer spacing was 1.42 nm for the GO membrane with a higher extent of oxidation. The membrane with higher extent of oxidation had a higher water permeability of 2.3 LMH/bar compared to 1.9 LMH/bar for the membrane with lower oxidation extent. Another important feature of their membranes was high GO loading of 500 mg/m^2, which was 8.3 times higher than GO loading for the membrane used in our study. Therefore, while analyzing their results, diffusion length was increased in proportion to GO loading with a reference value of the one optimized for our membranes and their reported interlayer spacing was used. We acknowledge that dimensions of GO sheets should have an impact on the overall diffusion length, however, no information on lateral dimensions of GO sheets was available. Relative charge densities of the membranes were estimated using the reported surface potential values and a reference value of the one optimized in this study, with the aid of Equation (10). It is interesting to note that the increase in sulfate removal is only around 5% for an operational water flux of 10 LMH under identical experimental conditions. Authors acknowledge that interlayer spacing of GO are subject to change with the change parameters, such as ionic strength and operating pressure. Incorporation of sensitivity of interlayer spacing to these parameters spacing could further improve the accuracy of the model.

4.7. Sensitivity to GO loading and effective interlayer spacing

A sensitivity analysis was performed by computing Na_2SO_4 rejection for rGO membranes by varying diffusion lengths and interlayer spacing, as shown in Fig. 7. Diffusion lengths of the GO membranes can be varied by changing the amount of GO deposited on the substrate. One can change interlayer spacing of GO-based membranes by modulating the O/C ratio of GO or confining the channels by crosslinking. Increasing diffusion lengths or decreasing interlayer spacing enhances diffusion/steric hindrance for ionic transport through the membrane and hence, higher retention of ions is expected. Furthermore, the desalination performance of the membrane is anticipated to be less sensitive to conditions affecting charge interactions, such as pH and feed concentration. Na_2SO_4 retention estimated for the rGO membranes with two different rGO loadings (24 and 120 mg/m^2) and two effective interlayer spacings (1.16 and 1.32 nm) at different pH (4 and 7) and feed concentrations (2 and 10 mM) is shown in SI Fig. S5. However, there exists a tradeoff between desalination performance and permeability of the rGO membranes. Permeability of the membrane scales inversely with the first power of the effective diffusion length and with the third power of the effective interlayer spacing according to the Hagen Poiseuille equation. A sensitivity analysis thus shows that a Nernst-Planck based mathematical approach could also be used to assess the enhanced desalination performance of GO-based membranes after increasing GO loading or decreasing effective interlayer spacing.

4.8. Produced water treatment

In this study, a potential nanofiltration-based application of rGO membranes for treatment of produced water was investigated with an objective to partially remove hardness and near

completely remove dissolved oil. Produced water samples used in the study had a total TDS content of 38800 mg/l. Water was mostly comprised of Na^+(14338 mg/l) and Cl^- (21990 mg/l) ions (SI Table S1). The water was estimated to have an osmotic pressure around 33 bar at 25 °C. The produced water flux through rGO and NF270 membranes was monitored at 10.3 bar. Filtration was operated in a cross-flow mode with permeate and retentate being recirculated to the feed to minimize the change in composition of the feed reservoir. For over 24 h of operation, no significant decay in flux was observed and both membranes retained salts partially (Fig. 8).

As expected, salt retention of both membranes was lower with a produced water than lower TDS experiments due to screening of the membrane charge at higher ionic strength. Reduction in produced water flux for both membranes is likely due to an osmotic pressure gradient caused by salt retention. Water flux estimated after osmotic pressure corrections was in close agreement with the observed produced water flux. Both membranes exhibited more than 90% flux recovery. High retention of dissolved oil by both the membranes was also observed. The concentration of dissolved oil was reduced from 26 ppm in the feed to <5 ppm (analytical method detection limit) in the permeates of both membranes. A TOC removal of 53% was observed (Fig. S6).

It is important to note the role of removal selectivity for the produced water application. A membrane with high TDS rejection, such as a seawater RO membrane, would have limited application. The high rejection of TDS would cause a high osmotic pressure difference requiring applied pressures beyond their operational limit. In additional, the high rejection of TDS would limit recovery due to the increased concentration of TDS in the concentrate. A selective membrane that allowed high passage of monovalent salts would have a significantly lower osmotic pressure difference across the membrane. It would also not increase the osmotic pressure significantly at increasing recoveries. This would allow low applied pressures despite the high TDS. Thus, a membrane with high selective of organics over TDS is a key element in determining the efficiency of separations.

4.9. Removal of perfluoro octanoic acid (PFOA) anion

In the case of organic anions, such as PFOA, repulsive charge interactions exist between the carboxylate functionalities of the molecules and the membrane surface. Therefore, one would expect that rGO and NF270 membranes would offer higher retention of these molecules compared to neutral solutes of similar size. The charge on these anions are expected to be more distributed compared to inorganic anions. Additionally, PFOA being a cylindrical molecule, relatively lower contribution of steric effects in the retention of these molecules compared to a branched molecule of similar molecular weight is anticipated. To understand the underlying exclusion mechanism for retention of PFOA, rejection tests were conducted at different feed recovery, operating pH and feed concentration in dead-end and cross-flow modes of operation.

Retention of PFOA by rGO membranes was evaluated at increasing water recovery up to 72% in a dead end mode of operation. The rejection of PFOA by rGO membranes and its concentration in the permeate for a 2.3 μM feed is shown in Fig. 9. The filtration concentrated the feed by 3.3 times. The error in the mass balance of the PFOA between the

initial feed and final streams (retentate and permeate) was less than 10%, ensuring accuracy of the results. Retention of PFOA by the rGO membrane is expected to be driven by charge and steric hindrance. For a charge-driven exclusion mechanism, retention is dependent on various parameters, such as feed ionic strength and pH. At higher feed concentrations, charge interactions between the solute and the membrane surface are suppressed, lowering its contribution to the resistance for PFOA transport through the membrane. The role of charge in the underlying mechanism was investigated by measuring PFOA retention by rGO membranes at a higher feed concentration of 46 μM. Constant rejection of around 60% was observed (Fig. 9a). The error in mass balance was less than 2%, indicating there was no significant adsorption of PFOA. Decrease in retention of PFOA at higher feed concentration (46 μM) suggests that charge plays a vital role in the exclusion mechanism. For real water samples, typical concentrations of PFAS are in trace levels (<50 ng/L) [40]. Based on the increased rejection at a lower feed concentration, significantly higher retention of PFAS by rGO membranes is expected at the low concentration levels in real water.

The impact of charge on the exclusion of PFOA by rGO membranes was further quantified by conducting a similar experiment at pH 3. At acidic pH, a decrease in retention of PFAS is expected due to a lower surface potential of the membrane. Also, PFOA has a pKa reported pKa value of 3.8 at infinite dilution, and thus, the influence of charge interactions in exclusion mechanism is further reduced [41]. A decrease in concentration of PFOA on the permeate side was observed, however, the retentate concentration after 75% recovery was the same as that of the feed (Fig. 9b). The lack of any change in the PFOA concentration on the retentate side at a lower pH implied adsorption of PFOA on the membrane surface [42,43]. It was, therefore, not confirmed whether the lower permeate concentration at acid pH was due to rejection or adsorption. Performance of the rGO membranes was also evaluated in a cross-flow mode of operation with 46 μM feed for over 24 h of operation. The membrane had a constant rejection percentage of 72%. Higher retention in a cross-flow mode compared to a dead-end mode of operation is expected due to a lower extent of concentration polarization.

Retention of PFOA by a commercial nanofiltration membrane, NF270 (DOW-FILMTEC), was also investigated. NF270 membranes exhibited 90% retention of PFOA at pH 7 for 46 μM feed. The observed error in mass balance was less than 5%, as shown in Fig. 9c. Retention of PFOA by NF270 membrane declined to 50% at pH 3. A significant decrease in PFOA retention by the NF270 at pH 3 likely indicates the existence of a charge-driven exclusion mechanism for these membranes as well. Our results are consistent with the findings of Elimelech et al. (2018), where the authors observed over 90% PFOA retention by a NF270 membrane for a 2.3 μM feed at pH 7 [18].

5. Conclusion

A modelling approach based on the extended Nernst-Planck equation was used to elucidate the role of steric hindrance and charge-based interactions in the overall exclusion of ions by rGO membranes. It was determined that rGO membrane's separation performance is primarily governed by charge interactions. Optimized parameters of the extended Nernst-Planck equation suggested rGO (60 mg/m^2 GO loading) has a larger pore opening (1.2

nm), a longer diffusion length (500 nm) and a higher effective charge density (−40 mol/m^3) than the NF270 (DOW-Filmtec) nanofiltration membrane (pore size: 0.86 nm, diffusion length: 50 nm, charge density: 26 mol/m^3). The impact of parameters (such as, diffusion length and interlayer spacing) influencing steric hindrance and charge interactions on the transport of solutes were quantified via sensitivity analysis. rGO membranes were found to partially remove hardness (13% Ca retention) from high TDS produced water along with high retention (74%) of dissolved oil (an organic impurity). These membranes were found to be suitable for the treatment of high TDS water with the goal of removing organic impurities since the osmotic pressure gradient is low. Exclusion of Perfluoroalkyl substances (PFAS) by rGO membranes was studied using perfluorooctanoic acid (PFOA) at various operating conditions with an impetus of elucidating the underlying exclusion mechanism. Membranes exhibited 80% removal of PFOA for 2.3 μM feed at pH 7. PFOA retention by rGO membranes was driven primarily by charge repulsion and steric hindrance.

Supplementary Material

Refer to Web version on PubMed Central for supplementary material.

Acknowledgement

This research was supported by the National Science Foundation under Cooperative Agreement No. 1355438, and by NIH-NIEHS-SRC (Award number: P42ES007380). GO Membrane development and produced water treatment aspects was funded by Chevron Corporation. Clair Jordon was supported by NSF-REU program. Authors also acknowledge the intellectual contributions made by Dr. Andrew Colburn in the analysis of membrane performance. The work was partially funded by the Australian Research Council Research Hub for Graphene Enabled Industry Transformation (IH150100003).

Abbreviations and Notations

A	Effective membrane or Orifice diameter area in membrane and diffusion cells (m^2)
$\mathbf{A_w}$	Water Permeability (LMH/bar)
B	Solute permeability (m/s)
$\mathbf{C_{per}}$	Solute concentration in permeate stream after membrane filtration (mol/m^3 or mM)
$\mathbf{C_{feed}}$	Solute concentration in feed solution (mol/m^3 or mM)
$\mathbf{C_{donor}}$	Concentration of solute in donor chamber of diffusion cell (mol/m^3 or mM)
$\mathbf{C_{collector}}$	Concentration of solute in collector chamber of diffusion cell (mol/m^3 or mM)
$\mathbf{D_i}$	Solute diffusivity (m^2/s)
$\mathbf{d_h}$	hydrated diameter of the solute (nm)

$\mathbf{F_{media}}$	Flow rate of circulating media in diffusion cell (μL/min or SI)
$\mathbf{F_s}$	Solute flow
$\mathbf{J_i}$	Solute flux (moles/m^2/sec)
$\mathbf{J_v}$	Water flux (LMH or Liters/m^2/hour)
$\mathbf{K_m}$	Mass transfer coefficient (Dimensionless)
$\mathbf{K_{di}}$	Hindered diffusion coefficient (Dimensionless)
$\mathbf{K_{ci}}$	Convective coupling coefficient (Dimensionless)
L	Diffusion length
R	Rejection or retention of solute by membranes
$\mathbf{R_c}$	Resistance of Graphene layer
$\mathbf{V_{donor}}$	Volume of donor chamber
$\mathbf{X_d}$	Membrane charge density (moles/m^3)
$\mathbf{Z_i}$	valence state of ions
ζ	Surface Zeta Potential
$\mathbf{d_\psi}$	Donnan potential across the membrane
$\boldsymbol{\tau}_{yx\|d}$	Shear stress
μ	Fluid viscosity
ΔP	Transmembrane pressure
Δπ	Transmembrane osmotic pressure gradient
α	Specific resistance of Graphene layers
R	Ideal gas constant (8.314 $JK^{-1}mol^{-1}$)
e	Electron charge (1.6×10^{-19} Coulombs)
$\mathbf{K_B}$	Boltzman constant (1.38×10^{-23} m^2 kg s^{-2} K^{-1})
F	Faraday constant (96485 s A/mol)
Na	Avogadro number (6.02×10^{-23} mol^{-1})

References

[1]. Zhang Y, Chung TS, Graphene oxide membranes for nanofiltration, Curr. Opin. Chem. Eng. 16 (2017) 9–15, 10.1016/j.coche.2017.03.002.

[2]. Jiang Y, Biswas P, Fortner JD, A review of recent developments in graphene-enabled membranes for water treatment, Environ. Sci.: Water Res. Technol. 2 (2016) 915–922, 10.1039/C6EW00187D.

[3]. Abraham J, Vasu KS, Williams CD, Gopinadhan K, Su Y, Cherian CT, Dix J, Prestat E, Haigh SJ, Grigorieva IV, Carbone P, Geim AK, Nair RR, Tunable sieving of ions using graphene oxide membranes, Nat. Nanotechnol. 12 (2017) 546–550, 10.1038/nnano.2017.21. [PubMed: 28369049]

[4]. Liu G, Jin W, Xu N, Graphene-based membranes, Chem. Soc. Rev. 44 (2015) 5016–5030, 10.1039/C4CS00423J.

[5]. Yuan Y, Gao X, Wei Y, Wang X, Wang J, Zhang Y, Gao C, Enhanced desalination performance of carboxyl functionalized graphene oxide nanofiltration membranes, Desalination 405 (2017) 29–39, 10.1016/j.desal.2016.11.024.

[6]. Chang Y, Shen Y, Kong D, Ning J, Xiao Z, Liang J, Zhi L, Fabrication of the reduced preoxidized graphene-based nanofiltration membranes with tunable porosity and good performance, RSC Adv 7 (2017) 2544–2549, 10.1039/C6RA24746F.

[7]. Aher A, Thompson S, Nickerson T, Ormsbee L, Bhattacharyya D, Reduced graphene oxide–metal nanoparticle composite membranes for environmental separation and chloro-organic remediation, RSC Adv. 9 (2019) 38547–38557, 10.1039/c9ra08178j. [PubMed: 32095233]

[8]. Bowen WR, Welfoot JS, Modelling the performance of membrane nanoÿltration — critical assessment and model development, Chem. Eng. Sci. 57 (2002) 1121–1137.

[9]. Lee CS, Choi MK, Hwang YY, Kim H, Kim MK, Lee YJ, Yun Jung L, Facilitated water transport through graphene oxide membranes functionalized with aquaporin-mimicking peptides, Adv. Mater. 30 (2018) 1–9, 10.1002/adma.201705944.

[10]. Akbari A, Meragawi S, Martin S, Corry B, Shamsaei E, Easton CD, Bhattacharyya D, Majumder M, Solvent transport behavior of shear aligned graphene oxide membranes and implications in organic solvent nanofiltration, ACS Appl. Mater. Interfaces (2017), 7b11777, 10.1021/acsami.7b11777acsami.

[11]. Yang E, Ham MH, Park HB, Kim CM, ho Song J, Kim IS, Tunable semipermeability of graphene-based membranes by adjusting reduction degree of laminar graphene oxide layer, J. Membr. Sci. 547 (2018) 73–79, 10.1016/j.memsci.2017.10.039.

[12]. Gogoi A, Konch TJ, Raidongia K, Anki Reddy K, Water and salt dynamics in multilayer graphene oxide (GO) membrane: role of lateral sheet dimensions, J. Membr. Sci. 563 (2018) 785–793, 10.1016/j.memsci.2018.06.031.

[13]. Anderson JL, Quinn JA, Restricted transport in small pores a model for steric exclusion and hindered particle motion, Biophys. J. 14 (1974) 130–150, 10.1016/S0006-3495(74)70005-4. [PubMed: 4813157]

[14]. Werber JR, Osuji CO, Elimelech M, Materials for next-generation desalination and water purification membranes, Nat. Rev. Mater. 1 (2016), 16018, 10.1038/natrevmats.2016.18.

[15]. Ahmadi A, Qanati O, Dorraji MSS, Rasoulifard MH, Vatanpour V, Investigation of antifouling performance a novel nanofibrous S-PVDF/PVDF and S-PVDF/PVDF/GO membranes against negatively charged oily foulants, J. Membr. Sci. 536 (2017) 86–97.

[16]. V Headley J, Peru KM, Barrow MP, Advances in mass spectrometric characterization of naphthenic acids fraction compounds in oil sands environmental samples and crude oil: a review, Mass Spectrom. Rev. 35 (2016) 311–328. [PubMed: 25970647]

[17]. Bach CC, Bech BH, Brix N, Nohr EA, Bonde JPE, Henriksen TB, Perfluoroalkyl and polyfluoroalkyl substances and human fetal growth: a systematic review, Crit. Rev. Toxicol. 45 (2015) 53–67, 10.3109/10408444.2014.952400. [PubMed: 25372700]

[18]. Boo C, Wang Y, Zucker I, Choo Y, Osuji CO, Elimelech M, High performance nanofiltration membrane for effective removal of Perfluoroalkyl substances at high water recovery, Environmental Science & Technology 52 (2018) 7279–7288, 10.1021/acs.est.8b01040. [PubMed: 29851340]

[19]. Hang X, Chen X, Luo J, Cao W, Wan Y, Removal and recovery of perfluorooctanoate from wastewater by nanofiltration, Separ. Purif. Technol. 145 (2015) 120–129, 10.1016/j.seppur.2015.03.013.

[20]. Aher A, Sarma R, Crocker M, Bhattacharyya D, Selective molecular separation of lignin model compounds by reduced graphene oxide membranes from solvent-water mixture, Separ. Purif. Technol. 230 (2020), 115865, 10.1016/j.seppur.2019.115865.

[21]. Córdoba-Diaz M, Nova M, Elorza B, Córdoba-Diaz D, Chantres JR, Córdoba-Borrego M, Validation protocol of an automated in-line flow-through diffusion equipment for in vitro permeation studies, J. Contr. Release 69 (2000) 357–367.

[22]. Grewer DM, Young RF, Whittal RM, Fedorak PM, Naphthenic acids and other acid-extractables in water samples from Alberta: what is being measured? Sci. Total Environ. 408 (2010) 5997–6010. [PubMed: 20825979]

[23]. Jivraj MN, MacKinnon M, Fung B, Naphthenic Acid Extraction and Quantitative Analysis with FT-IR Spectroscopy, Syncrude Analytical Manuals, 1995.

[24]. Garcia-Aleman J, Dickson JM, Mathematical modeling of nanofiltration membranes with mixed electrolyte solutions, J. Membr. Sci. 235 (2004) 1–13, 10.1016/j.memsci.2003.11.023.

[25]. Maria A, Alves B, Computer program for simulation of mass transport in nanofiltration membranes 321 (2008) 172–182, 10.1016/j.memsci.2008.04.054.

[26]. Bowen WR, Mohammad AW, Hilal N, Characterisation of nanofiltration membranes for predictive purposes - use of salts, uncharged solutes and atomic force microscopy, J. Membr. Sci. 126 (1997) 91–105, 10.1016/S0376-7388(96)00276-1.

[27]. Deen WM, Hindered transport of large molecules in liquid-filled pores, AIChE J 33 (1987) 1409–1425, 10.1002/aic.690330902.

[28]. Aher A, Cai Y, Majumder M, Bhattacharyya D, Synthesis of graphene oxide membranes and their behavior in water and isopropanol, Carbon 116 (2017) 145–153, 10.1016/j.carbon.2017.01.086. [PubMed: 31130736]

[29]. Wadekar SS, Vidic RD, Influence of active layer on separation potentials of nanofiltration membranes for inorganic ions, Environmental Science & Technology (2017), 10.1021/acs.est.6b05973acs.est.6b05973.

[30]. Han Y, Xu Z, Gao C, Ultrathin graphene nanofiltration membrane for water purification, Adv. Funct. Mater. 23 (2013) 3693–3700, 10.1002/adfm.201202601.

[31]. Akbari A, Sheath P, Martin ST, Shinde DB, Shaibani M, Banerjee PC, Tkacz R, Bhattacharyya D, Majumder M, Large-area graphene-based nanofiltration membranes by shear alignment of discotic nematic liquid crystals of graphene oxide, Nat. Commun. 7 (2016), 10891, 10.1038/ncomms10891. [PubMed: 26947916]

[32]. Nightingale ER, Phenomenological theory of ion solvation. Effective radii of hydrated ions, J. Phys. Chem. 63 (1959) 1381–1387, 10.1021/j150579a011.

[33]. Tansel B, Sager J, Rector T, Garland J, Strayer RF, Levine L, Roberts M, Hummerick M, Bauer J, Significance of hydrated radius and hydration shells on ionic permeability during nanofiltration in dead end and cross flow modes, Separ. Purif. Technol. 51 (2006) 40–47, 10.1016/j.seppur.2005.12.020.

[34]. Richards LA, Schãfer AI, Richards BS, Corry B, The importance of dehydration in determining ion transport in narrow pores, Small 8 (2012) 1701–1709, 10.1002/smll.201102056. [PubMed: 22434668]

[35]. Ritt C, Werber JR, Deshmukh A, Elimelech M, Monte Carlo simulations of framework defects in layered two-dimensional nanomaterial desalination membranes: implications for permeability and selectivity, Environmental Science & Technology (2019), 10.1021/acs.est.8b06880acs.est.8b06880.

[36]. Erickson K, Erni R, Lee Z, Alem N, Gannett W, Zettl A, Determination of the local chemical structure of graphene oxide and reduced graphene oxide, Adv. Mater. 22 (2010) 4467–4472, 10.1002/adma.201000732. [PubMed: 20717985]

[37]. Childress AE, Elimelech M, Relating nanofiltration membrane performance to membrane charge (electrokinetic) characteristics, Environ. Sci. Technol. 34 (2000) 3710–3716, 10.1021/es0008620.

[38]. Colburn AS, Meeks N, Weinman ST, Bhattacharyya D, High total dissolved solids water treatment by charged nanofiltration membranes relating to power plant applications, Ind. Eng. Chem. Res. 55 (2016) 4089–4097, 10.1021/acs.iecr.6b00098. [PubMed: 31130776]

[39]. Aher A, Papp J, Colburn A, Wan H, Hatakeyama E, Prakash P, Weaver B, Bhattacharyya D, Naphthenic acids removal from high TDS produced water by persulfate mediated iron oxide functionalized catalytic membrane, and by nanofiltration, Chem. Eng. J. 327 (2017) 573–583, 10.1016/j.cej.2017.06.128. [PubMed: 29398952]

[40]. Suja F, Pramanik BK, Zain SM, Contamination, bioaccumulation and toxic effects of perfluorinated chemicals (PFCs) in the water environment: a review paper, Water Sci. Technol. 60 (2009) 1533–1544. [PubMed: 19759456]

[41]. Burns DC, Ellis DA, Li H, McMurdo CJ, Webster E, Experimental p K a determination for perfluorooctanoic acid (PFOA) and the potential impact of p K a concentration dependence on laboratory-measured partitioning phenomena and environmental modeling, Environmental Science & Technology 42 (2008) 9283–9288. [PubMed: 19174905]

[42]. Gao X, Chorover J, Adsorption of perfluorooctanoic acid and perfluorooctanesulfonic acid to iron oxide surfaces as studied by flow-through ATR-FTIR spectroscopy, Environ. Chem 9 (2012) 148–157.

[43]. Bei Y, Deng S, Du Z, Wang B, Huang J, Yu G, Adsorption of perfluorooctane sulfonate on carbon nanotubes: influence of pH and competitive ions, Water Sci. Technol. 69 (2014) 1489–1495. [PubMed: 24718341]

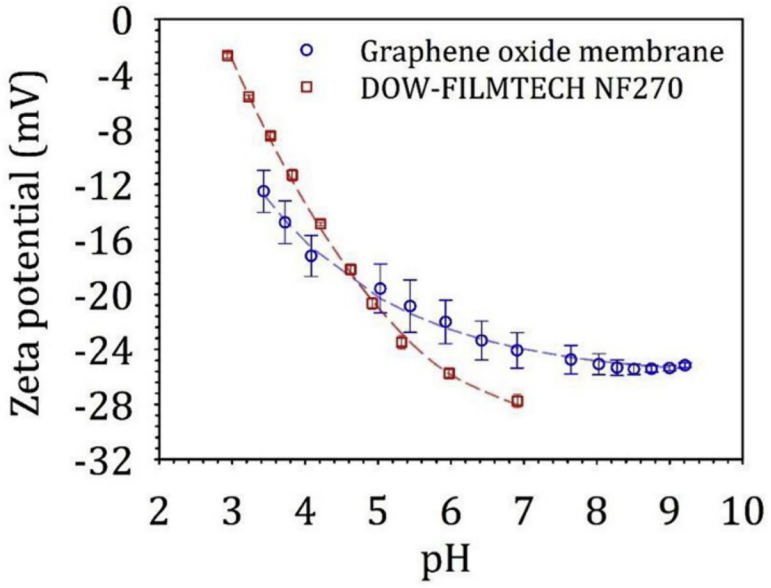

Fig. 1.
Zeta potential of Graphene Oxide membranes measured using 0.01 M KOH as electrolyte.

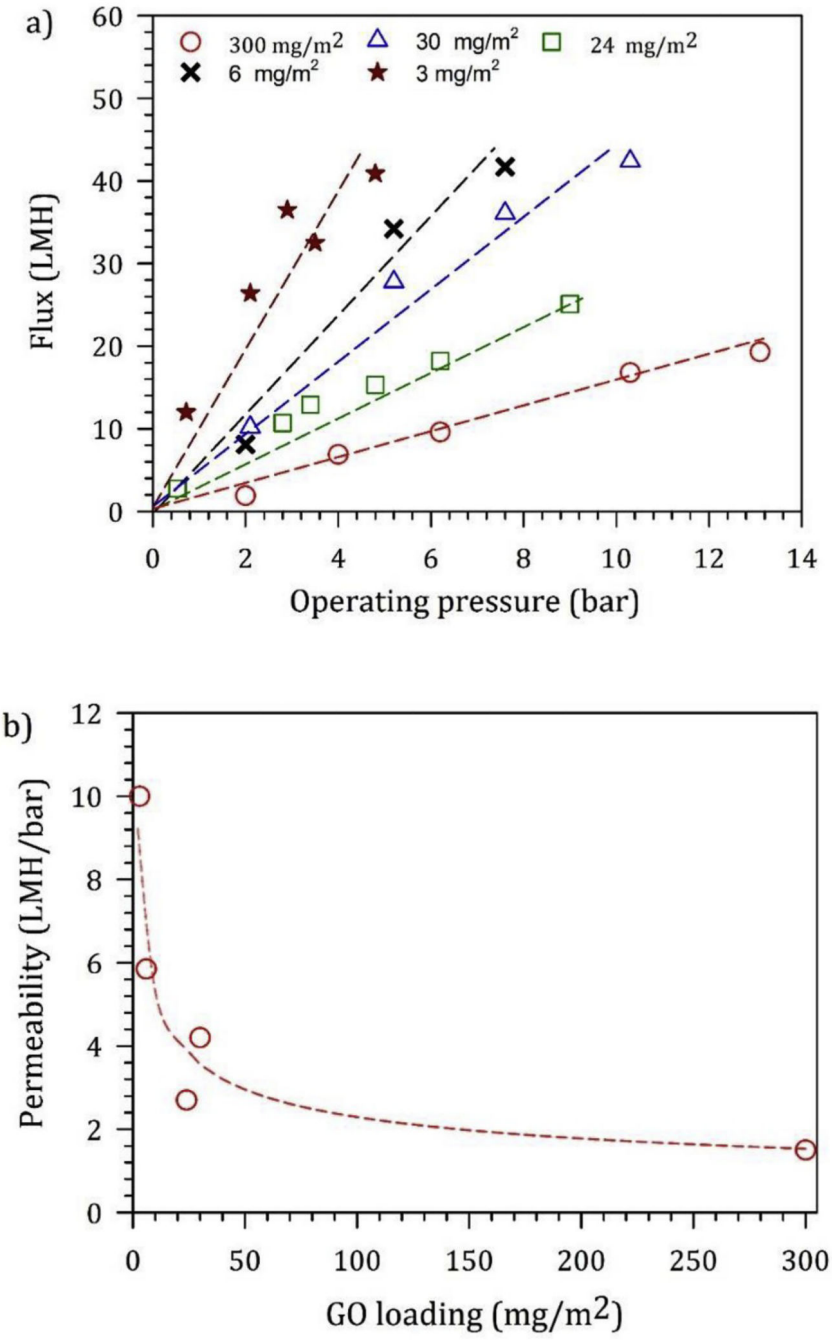

Fig. 2.

a) Flux-pressure dependence and b) Permeability of GO membranes with different loadings of Graphene Oxide (tested for pressure up to 13 bar).

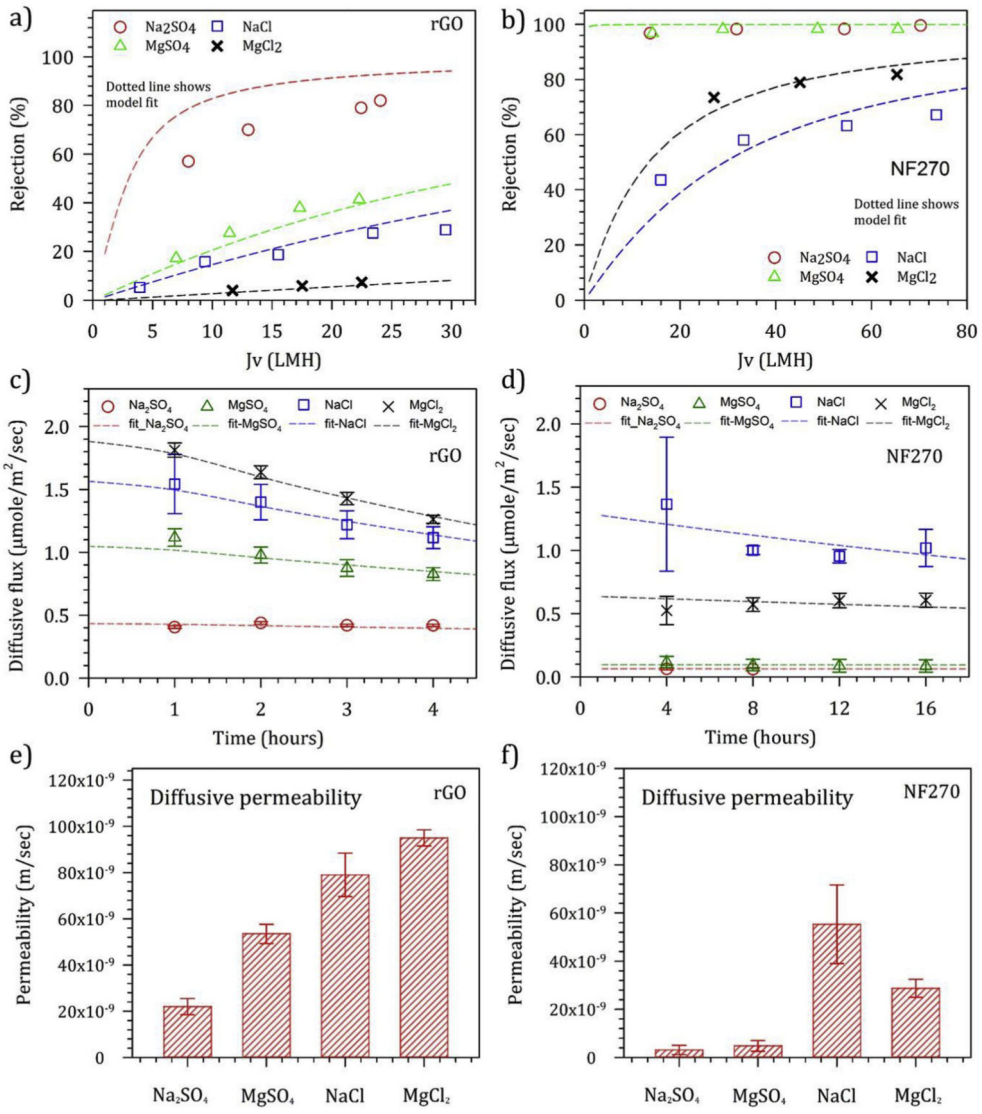

Fig. 3.

Retention and diffusive permeability of different salts through rGO (a, c and e) and NF270 membranes (b, d and f). rGO loading: 60 mg/m^2, Salts: Na_2SO_4, $MgSO_4$, $MgCl_2$, NaCl. Retentions and diffusive permeabilities measured at 5 and 10 mM feed concentration, respectively. Temp: 25 °C, pH: 7.

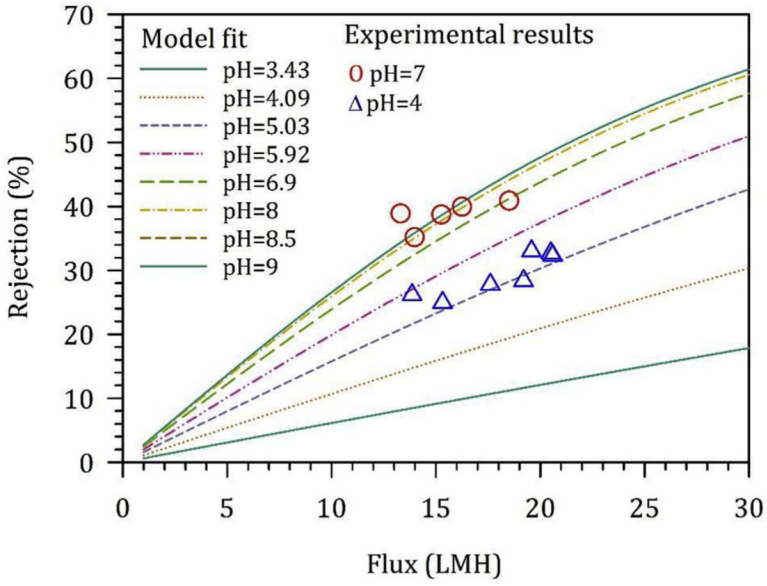

Fig. 4.

Influence of pH on transport of sodium sulfate through the Graphene Oxide membrane. GO loading: 120 mg/m^2, pure water permeability: 2 LMH/bar, [Na_2SO_4] = 20 mM. Cross-flow mode of operation, Crossflow velocity: 0.7 m/s, Temp: 23 °C.

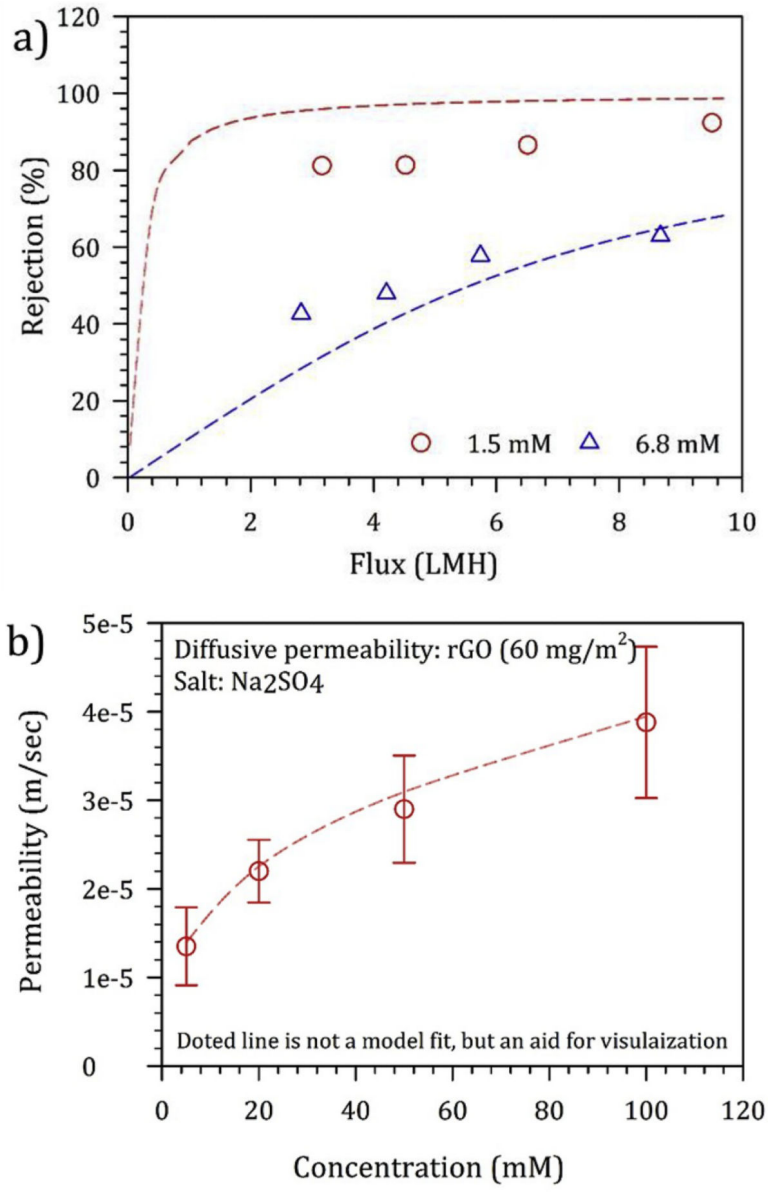

Fig. 5.

Role of ionic strength on transport of Na_2SO_4 through rGO membrane. **a)** Na_2SO_4 rejection. GO loading: 60 mg/m^2, pure water permeability: 2 LMH/bar, Cross-flow mode of operation, Crossflow velocity: 0.7 M/s, Temp: 23 °C. Solid line shows results obtained from Nernst-Planck equation based model. **b)** diffusive permeability of Na_2SO_4 through rGO membranes.

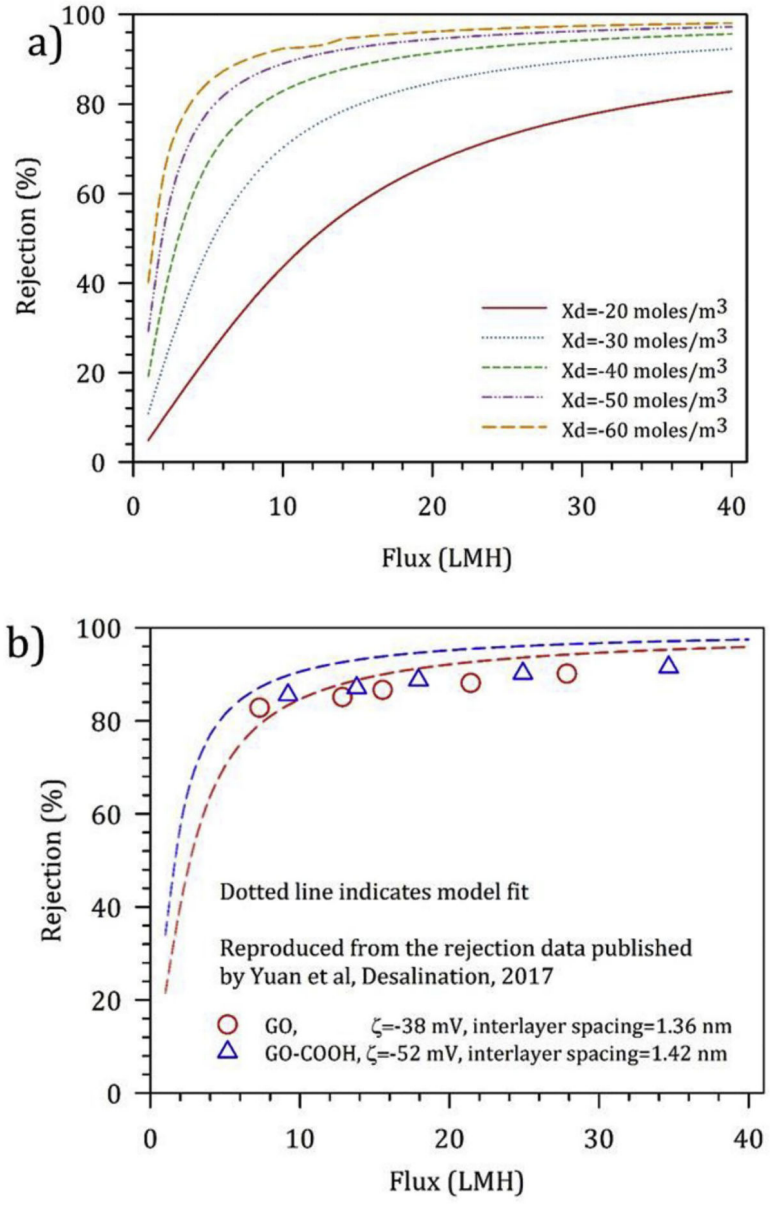

Fig. 6.

Sensitivity of the desalination performance of GO membranes to the effective charge density, **a)** Sensitivity analysis was performed by varying charge density for the GO membranes (60 mg/m^2) used in this study, feed [Na_2SO_4] = 5 mM, Temp = 23 °C, **b)** Analysis of Na_2SO_4 rejection data published by Yuan et al. for GO membranes with different extent of oxidation (Reproduced from [dummy_]Fig. 12 c and d, Yuan et al. Desalination 405 (2017) 29–39): Experimental conditions: GO loading = 500 mg/m^2, feed [Na_2SO_4] = 13.6 mM, Mode of operation: Cross-flow, Cross-flow velocity: 5 m/s, permeability of GO membranes: 1.9 (lower extent of oxidation) and 2.3 LMH/bar (higher extent of oxidation). Model fit parameters: L = 4.15 μm, Xd = −67 mol/m^3 for GO and −99 mol/m^3 for GO-COOH membranes, rp = 0.68 nm for GO and 0.71 nm for GO-COOH membranes.

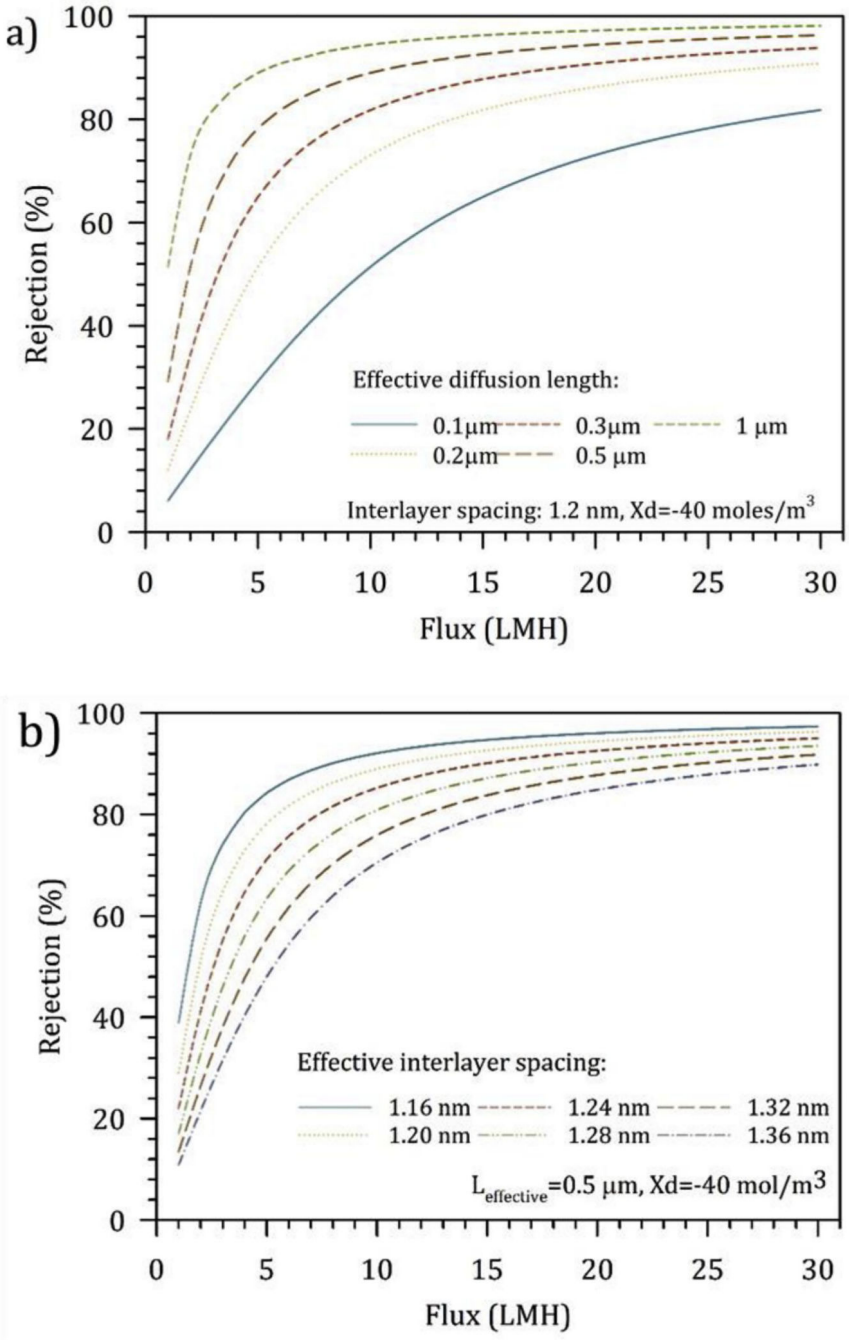

Fig. 7.

Sensitivity analysis to quantify the impact of effective diffusion length and interlayer spacing of GO membranes on retention of Na_2SO_4 (C_{feed}: 5 mM).

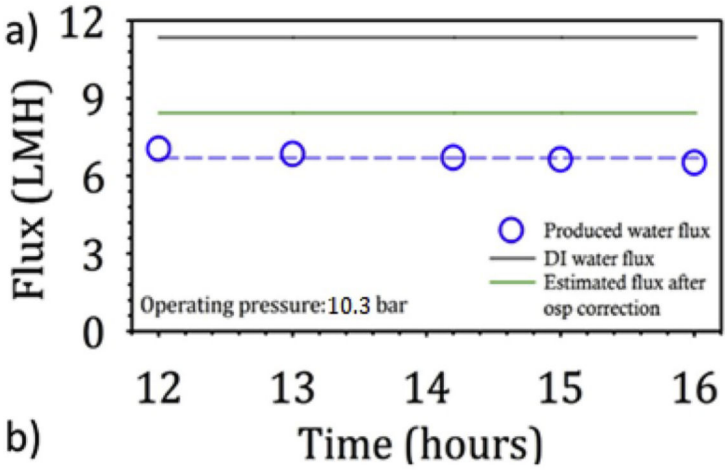

	GO	NF270
Produced water flux	7 LMH	28 LMH
Operating Pressure	10.3 bar	10.3 bar
Ca removal (500 ppm in Feed)	14%	31%
Na removal (14,500 ppm in Feed)	9%	7%
Dissolved oil removal	74%	72%

Fig. 8.

a) Produced water flux by rGO membrane and b) salt retention.

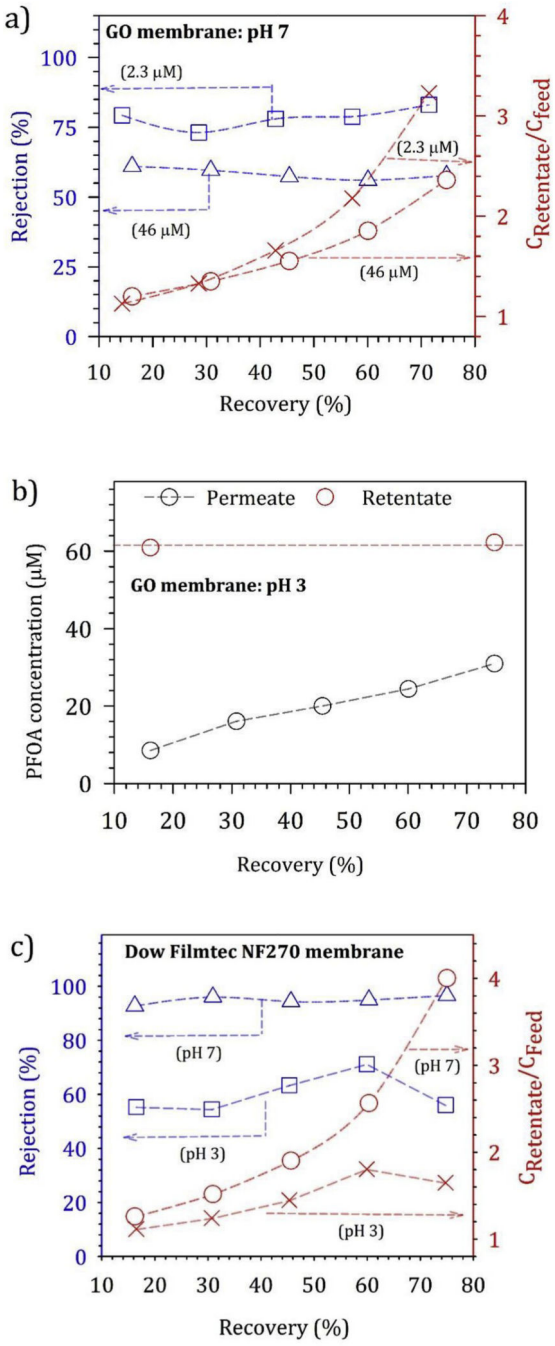

Fig. 9.

PFOA retention by rGO membranes and NF270 membranes with increasing recovery. A) PFOA retention by GO membranes for 1 ppm and 20 ppm feed concentration at pH 7, b) PFOA retention by GO membranes for 20 ppm feed concentration at pH 3 and c) PFOA retention by NF270 membrane for 20 ppm feed at pH 3 and pH 7.

Table 1

Properties of ions investigated in the study[a].

Ions/Solutes	Diffusivity (m^2s^{-1})$^{a}10^{-9}$	Hydrated radius (nm)
Na^+	1.33	0.36
Mg^{2+}	0.72	0.43
Cl^-	2.03	0.33
SO_4^{2-}	1.06	0.38

[a]Diffusivity and hydrated radius values were adapted from Bowen et al. Chemical Engineering Science, 2002 and E.R. Nightingale, Journal of Physical Chemistry, 1959., respectively.

Table 2

Optimized membrane parameters for salt retention by rGO and NF270 membranes using the extended Nernst-Planck equation.

Membrane	**rGO (Loading: 60 mg/m^2)**	**NF270**
Pure water permeability (LMH/bar)	1.6	14
Pore size (pore diameter/channel spacing, nm)	1.2	0.86
X_d (charge density, moles/m^3)	−40	−26
ΔX (nm) (Effective diffusion length, nm)	500	55